

# Study of fluorescence quenching due to 2, 3, 5, 6-tetrafluoro-7, 7', 8, 8'-tetracyano quinodimethane and its solid state diffusion analysis using photoluminescence spectroscopy

Priyanka Tyagi,<sup>1,2,a)</sup> Suneet Tuli,<sup>2</sup> and Ritu Srivastava<sup>1,b)</sup>

<sup>1</sup>CSIR-National Physical Laboratory, Physics of Energy Harvesting Division, CSIR-Network of Institute for Solar Energy (NISE), Dr. K.S.Krishnan Road, New Delhi 110012, India

<sup>2</sup>Center for Applied Research in Electronics, Indian Institute of Technology Delhi, New Delhi 110016, India

(Received 24 August 2014; accepted 20 January 2015; published online 6 February 2015)

In this work, we have studied the fluorescence quenching and solid state diffusion of 2, 3, 5, 6-tetrafluoro-7, 7', 8, 8'-tetracyano quinodimethane (F<sub>4</sub>-TCNQ) using photoluminescence (PL) spectroscopy. Quenching studies were performed with tris (8-hydroxyquinolino) aluminum (Alq<sub>3</sub>) in solid state samples. Thickness of F<sub>4</sub>-TCNQ was varied in order to realize different concentrations and study the effect of concentration. PL intensity has reduced with the increase in F<sub>4</sub>-TCNQ thicknesses. Stern-Volmer and bimolecular quenching constants were evaluated to be 13.8 M<sup>-1</sup> and 8.7 × 10<sup>8</sup> M<sup>-1</sup> s<sup>-1</sup>, respectively. The quenching mechanism was found to be of static type, which was inferred by the independent nature of excited state life time from the F<sub>4</sub>-TCNQ thickness. Further, solid state diffusion of F<sub>4</sub>-TCNQ was studied by placing a spacing layer of α-NPD between F<sub>4</sub>-TCNQ and Alq<sub>3</sub>, and its thickness was varied to probe the diffusion length. PL intensity was found to increase with the increase in this thickness. Quenching efficiency was evaluated as a function of distance between F<sub>4</sub>-TCNQ and Alq<sub>3</sub>. These studies were performed for the samples having 1, 2.5, and 5.5 nm thicknesses of F<sub>4</sub>-TCNQ to study the thickness dependence of diffusion length. Diffusion lengths were evaluated to be 12.5, 15, and 20 nm for 1, 2.5, and 5.5 nm thicknesses of F<sub>4</sub>-TCNQ. These diffusion lengths were found to be very close to that of determined by secondary ion mass spectroscopy technique. © 2015 AIP Publishing LLC. [<http://dx.doi.org/10.1063/1.4907274>]

## INTRODUCTION

Organic semiconductors have become imperative element for modern and future era electronic and optoelectronic devices such as organic light emitting diodes (OLEDs), organic photovoltaics (OPVs), organic field effect transistors (OFETs), and organic sensors.<sup>1-4</sup> A variety of novel materials and processes have been developed and implemented in these devices over the past 20 years, due to which, the field of organic electronics has rapidly progressed.<sup>5-9</sup> Fluorescence quenching is one of the techniques, which has been frequently utilized, in order to develop these devices.<sup>10-14</sup> 2,3,5,6-tetrafluoro-7,7',8,8'- tetracyano quinodimethane (F<sub>4</sub>-TCNQ) has found its versatility in all of these devices due to its capability of forming charge transfer (CT) complex and quenching of fluorescence.<sup>15-19</sup> F<sub>4</sub>-TCNQ possesses high electron affinity, which makes it highly suitable p-type dopant and has been found applicable for most of the hole transport materials.<sup>20</sup> F<sub>4</sub>-TCNQ has been widely studied; still, there are some major properties of F<sub>4</sub>-TCNQ need to be fully understood, which includes the fluorescence quenching and solid state diffusion.

F<sub>4</sub>-TCNQ has a strong electron accepting nature, therefore, it forms charge transfer complex with most of the organic molecules,<sup>20</sup> and this formation of charge transfer complex is

beneficial for the enhancement of conductivity (by increasing carrier concentration) in hole transport materials, however, the same concept originates the fluorescence quenching in emitting molecule.<sup>15-20</sup> Fluorescence quenching is beneficial in some cases such as OPVs but detrimental in OLEDs.<sup>20</sup> There are many reports on the potential use of F<sub>4</sub>-TCNQ; however, the quenching mechanism due to F<sub>4</sub>-TCNQ is still unknown. Although, devices utilize the solid state form of materials, most of the quenching studies on different fluorophore—quencher systems were performed in solution.<sup>21-24</sup> These studies are questionable for their direct applicability to the devices because the quencher has more degree of freedom to interact with fluorophore in solution in comparison to the solid state form. Therefore, quenching studies need to be performed in solid state form for their direct applicability in the devices.

There are many types of quenching mechanisms observed in various systems.<sup>21-24</sup> These include static quenching, dynamic quenching, and resonant energy transfer.<sup>25</sup> Among these mechanisms, static and dynamic quenchings are frequently observed, in case of the systems having charge transfer as the cause for fluorescence quenching. Static quenching occurs when a stable charge transfer complex is formed between the fluorophore and quencher in ground state, and if this complex is non-radiative, the photoluminescence (PL) intensity of fluorophore is statically quenched.<sup>26</sup> Dynamic or collisional quenching is observed when the excited state of fluorophore comes in contact with the quencher or the charge transfer complex is formed in the excited state, which facilitates

<sup>a)</sup>priyanka.tyagi.193@gmail.com

<sup>b)</sup>Author to whom correspondence should be addressed. Electronic mail: ritu@nplindia.org; Telephone: 91-11-45608596.

the non-radiative decay.<sup>27</sup> Dynamic quenching reduces the excited state life time of fluorophore, and it is dependent on the concentration of quencher; however, in case of static quenching, it remains unaffected.<sup>26,27</sup>

Further, F<sub>4</sub>-TCNQ has a proclivity towards diffusion in solid state form, which affects the device properties drastically. Diffusion is generally defined as a tendency to migration of neutral or ionized molecules inside the adjacent layers due to a concentration gradient. This diffusion generally happens at high temperatures; however, in case of F<sub>4</sub>-TCNQ, it is observed at room temperatures due to its low sticking coefficient with commonly used substrates.<sup>28,29</sup> When it is used as hole injection layer in OLEDs, its diffusion in hole transport layer was found to increase the conductivity of hole transport layer, and its diffusion in emissive layer was found to decrease the operational life time of OLEDs.<sup>28</sup> X-ray photo electron spectroscopy (XPS) and secondary ion mass spectroscopy (SIMS) have been used to study the solid state diffusion in context of inorganic and microelectronic devices.<sup>30,31</sup> SIMS has remained, by far, ahead of XPS for the diffusion studies due to its advantage of better spatial and depth resolution along with the high mass resolution and ability to differentiate between two molecules. However, SIMS is a destructive technique and requires more optimizations before its potential use. Furthermore, SIMS requires the etching of organic soft materials before its detection, which is very fast. Therefore, new methods are required to study solid state diffusion of F<sub>4</sub>-TCNQ. Since F<sub>4</sub>-TCNQ causes the fluorescence quenching in solid state, its diffusion can be studied by fluorescence measurements by proper design and optimization of experiments.

In this work, the quenching mechanism of F<sub>4</sub>-TCNQ was studied using steady state and time resolved PL spectroscopy. Sample architecture was designed and optimized to study the solid state diffusion of F<sub>4</sub>-TCNQ using PL spectroscopy.

## EXPERIMENTAL

Samples were prepared on glass substrate, which were cleaned sequentially by deionised water, acetone, trichloroethylene, and iso-propanol for 20 min in each using an ultrasonic bath. The sample configurations were

1. glass/F<sub>4</sub>-TCNQ (x nm)/Alq<sub>3</sub> (10 nm) for quenching studies,
2. glass/F<sub>4</sub>-TCNQ (x nm)/ $\alpha$ -NPD (y nm)/Alq<sub>3</sub> (10 nm) for diffusion studies,

where x and y were varied. F<sub>4</sub>-TCNQ,  $\alpha$ -NPD, and Alq<sub>3</sub> (purchased from Sigma Aldrich) were used as quencher, spacer, and fluorophore, respectively. Figs. 1(a) and 1(b) read the schematic illustrations of these configurations. The layers were deposited in a vacuum thermal evaporator system at a base pressure of  $4 \times 10^{-6}$  torr. F<sub>4</sub>-TCNQ layer was deposited at a rate of 0.1 Å/s, whereas other organic layers were deposited at a rate of 0.4 Å/s. The rates of evaporation were monitored *in situ* by using quartz crystal monitor. Steady state and time resolved photoluminescence spectrum was recorded using Fluorolog (Jobin Yvon-Horiba, model-3-11) spectrofluorometer at room temperature. In time resolved PL spectra (TRPL) films were excited using 405 nm nano LED

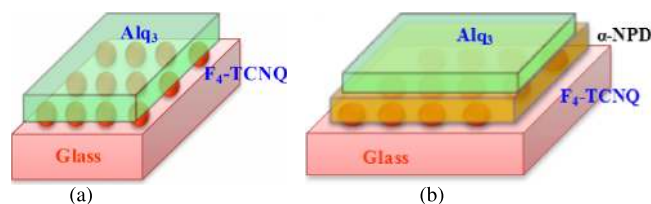


FIG. 1. Schematic illustration of the sample configurations used for (a) quenching studies and (b) diffusion studies of F<sub>4</sub>-TCNQ.

with pulse width of 1 ns. Absorption spectrum was measured using UV-Vis spectrophotometer model no. UV-2401 PV.

## RESULTS AND DISCUSSION

PL samples were fabricated with different thicknesses of F<sub>4</sub>-TCNQ and 10 nm thickness of Alq<sub>3</sub>. Alq<sub>3</sub> has a broad absorption spectrum ranging from 360–420 nm wavelengths and F<sub>4</sub>-TCNQ has narrow peak of absorption at 391 nm. PL samples were excited at 405 nm wavelength to avoid the simultaneous excitation of F<sub>4</sub>-TCNQ and Alq<sub>3</sub> because F<sub>4</sub>-TCNQ has a negligible absorption at this wavelength. Figure 2 illustrates the PL spectrum of samples with 0.5, 1, 1.5, and 2.5 nm thicknesses of F<sub>4</sub>-TCNQ. Thickness of F<sub>4</sub>-TCNQ was varied in these samples to realize different concentrations of F<sub>4</sub>-TCNQ in solid state, which is directly utilized in the device application. It can be seen from the figure that the peak PL intensity has reduced with the increase of the thickness of F<sub>4</sub>-TCNQ. The inset of Fig. 2 also shows the PL spectrum of the sample without F<sub>4</sub>-TCNQ. The peak PL intensities were found to be  $1.25 \times 10^7$ ,  $1.6 \times 10^6$ ,  $1.5 \times 10^6$ ,  $1.2 \times 10^6$ , and  $0.78 \times 10^6$  (a.u.) for 0, 0.5, 1.0, 1.5, and 2.5 nm thicknesses of F<sub>4</sub>-TCNQ, respectively. When Alq<sub>3</sub> is optically excited, electrons move from HOMO to LUMO state. Excited electrons form an excited bound state (exciton) with holes after losing some energy, known as exciton binding energy. This exciton decays radiatively to emit photon. Figure 3(a) illustrates the typical mechanism responsible for the decrease in PL intensity

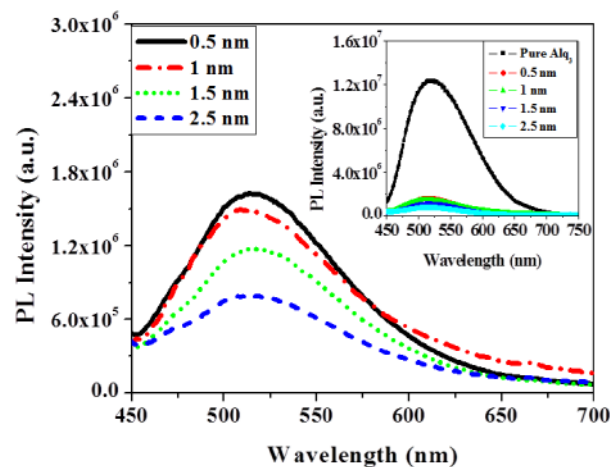


FIG. 2. PL spectrum of the samples with 0.5, 1, 1.5, and 2.5 nm thicknesses of F<sub>4</sub>-TCNQ and 10 nm thickness of Alq<sub>3</sub>. Inset also includes the PL spectrum of Alq<sub>3</sub> without F<sub>4</sub>-TCNQ layer.

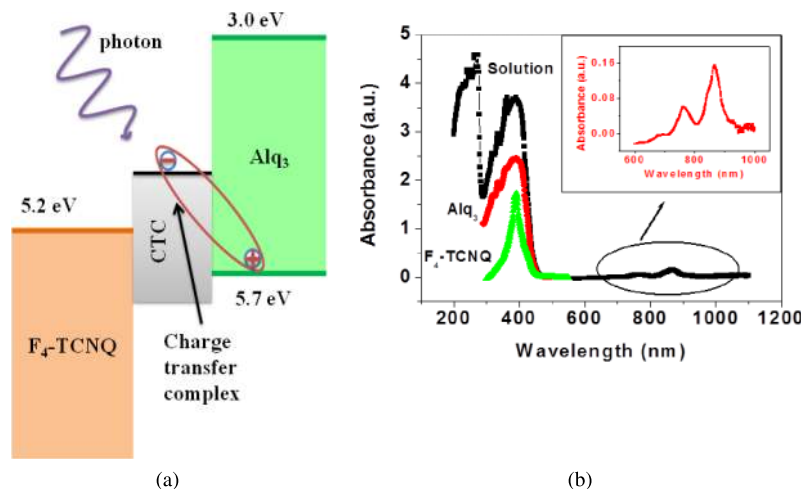
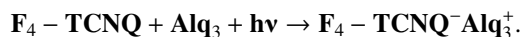


FIG. 3. (a) Schematic showing the hybrid charge transfer between  $F_4$ -TCNQ and  $Alq_3$ . (b) UV-Vis absorption spectrum of  $Alq_3$  +  $F_4$ -TCNQ and in chloroform having 0.36 mM and 2.2 mM concentrations. Figure also includes the absorption spectrum of  $Alq_3$  and  $F_4$ -TCNQ. Inset shows the magnified view of peaks at higher wavelength regime, arising due to the charge transfer between  $Alq_3$  and  $F_4$ -TCNQ.

in the samples with  $F_4$ -TCNQ, and it dissociates the exciton formed in  $Alq_3$  layer by accepting the electron from the bound state. The mechanism relies on the formation of hybrid charge transfer complexes upon the interaction of the donor and acceptor as also observed in case of P3HT and  $F_4$ -TCNQ.<sup>35</sup> In this case, the absorption cutoff of the charge transfer complex occurs at higher energies than in case of complete charge transfer where it is the difference between HOMO of donor and LUMO of acceptor



This mechanism was confirmed by measuring the absorption spectrum, a solution of  $F_4$ -TCNQ and  $Alq_3$  in chloroform having 0.36 mM and 2.2 mM concentration, respectively, which is shown in Fig. 3(b). This absorption spectrum has additional peaks at 760 and 860 nm, which correspond to energies 1.6 and 1.44 eV, respectively.  $Alq_3$  and  $F_4$ -TCNQ have their absorption peaks of around 360–420 nm and 391 nm wavelengths, respectively, corresponding to the  $\pi$ - $\pi^*$  transitions in their pristine forms (also shown in Fig. 3(b)). Therefore, these additional peaks cannot be associated to  $\pi$ - $\pi^*$  transitions of both  $F_4$ -TCNQ and  $Alq_3$  and have been associated to the formation of charge transfer complex between  $Alq_3$  and  $F_4$ -TCNQ as also observed in similar system by Wei *et al.*<sup>32</sup> The onset of charge transfer complex is 1.2 eV and higher than energy difference between the donor HOMO and acceptor LUMO which also indicates that the charge transfer between  $Alq_3$  and  $F_4$ -TCNQ is partial, and the difference between the donor HOMO and intermediate charge transfer complex LUMO is 1.2 eV. Further, the absorption spectra were measured for different concentrations of  $F_4$ -TCNQ in  $Alq_3$  in order to obtain detailed information about charge transfer complex. The used concentrations of  $F_4$ -TCNQ were 1, 2, 3, 4, 5, and 6 mM in 1 mM of  $Alq_3$ . The concentration of acceptor was selected to be higher in comparison to the donor to employ Benesi-Hildebrand method.<sup>33,34</sup> The charge transfer peak intensity has increased with the increase in the  $F_4$ -TCNQ concentration. Benesi-Hildebrand method has been employed in order to obtain a one to one binding analysis between acceptor and donor. In this method,  $[D]/Abs$  is plotted against  $1/[A]$ , where  $[D]$  is the donor concentration,  $[A]$  is the acceptor concentration, and  $Abs$  is the peak absorbance of

CT complex. Figure 4 depicts this plot, which exhibits a linear scaling with a slope of  $1/k\varepsilon$  and an intercept of  $1/\varepsilon$ , where  $\varepsilon$  is the molar absorptivity and  $k$  is the CT complex formation constant. This linear dependence also confirms complex formation between  $Alq_3$  and  $F_4$ -TCNQ. The values of  $\varepsilon$  and  $k$  were determined from the linear fit of the plot and were found to be  $5.8 \times 10^2 \text{ M}^{-1} \text{ cm}^{-1}$  and  $93.85 \text{ M}^{-1}$ , respectively. Similar CT complex studies on other systems ( $PVP-C_{60}$  and  $NMP-C_{60}$ ) have revealed significantly lower values of CT complex formation constants  $5.23 \text{ M}^{-1}$  and  $20.64 \text{ M}^{-1}$  for 1:1 complex in  $NMP-C_{60}$  and  $PVP-C_{60}$  systems.<sup>36</sup> This shows that the  $Alq_3$ - $F_4$ -TCNQ system has higher probability of CT-complex formation in comparison to these systems. The absorption spectrum analysis reveals that charge transfer complex is formed between  $Alq_3$  and  $F_4$ -TCNQ with a very high complex formation constant. This charge transfer complex is responsible for the reduction of PL intensity of  $Alq_3$  upon introduction of  $F_4$ -TCNQ.

Generally, the photo induced charge transfer from excited emitting molecule to the acceptor is very fast, therefore, the excitons inside  $Alq_3$  are more likely to be dissociated via charge transfer before the radiative decay. As the thickness of  $F_4$ -TCNQ has increased in our samples, the PL intensity has

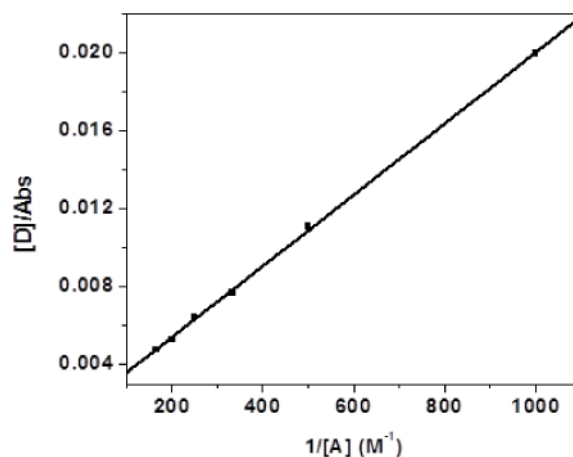


FIG. 4. Benesi-Hildebrand plot between  $[D]/Abs$  and  $1/[A]$  for the solution of  $Alq_3$  and  $F_4$ -TCNQ in chloroform showing a linear dependence.

reduced further. This may be ascribed as due to the increase in the concentration of accepting ( $F_4$ -TCNQ) molecules, which will increase the probability of exciton dissociation, thereby decreasing the PL intensity. The decreasing pattern of PL intensity was observed up to 2.5 nm thickness of  $F_4$ -TCNQ and further increase in the thickness has not decreased the PL intensity. This may be ascribed to the saturation in the formation of charge transfer complex between  $Alq_3$  and  $F_4$ -TCNQ.

Generally, PL quenching process, in case of charge transfer, is governed by the Stern-Volmer equation, which is given as

$$\frac{I_0}{I} = 1 + K_{sv} [Q], \quad (1)$$

where  $I_0$  and  $I$  are the emission intensities in the absence and presence of the quencher, respectively,  $K_{sv}$  is Stern-Volmer constant, and  $[Q]$  is the molar concentration of quencher. Molar concentration of  $F_4$ -TCNQ was calculated in our samples by using the following equation:

$$[Q] = \frac{\frac{\text{Mass of } F_4\text{-TCNQ (in gm)}}{\text{M.W. of } F_4\text{-TCNQ}}}{\text{Total volume (in litres)}}. \quad (2)$$

M.W. of  $Alq_3$  and  $F_4$ -TCNQ are 459.43 and 276.15 amu, respectively. Mass of  $F_4$ -TCNQ deposited on substrate was calculated by multiplying the volume of the film (cross-sectional area of the sample multiplied by thickness of  $F_4$ -TCNQ) with density of  $F_4$ -TCNQ ( $1.57 \text{ gm/cm}^3$ ). Total volume was first determined by using the total thickness (thickness of  $F_4$ -TCNQ + Thickness of  $Alq_3$ ) deposited in each sample and cross-sectional area of the sample in  $\text{cm}^3$  and then converted into liters by using standard conversion. Equation (2) is valid when quencher ( $F_4$ -TCNQ) is homogeneously dispersed in the host ( $Alq_3$ ) and to confirm this, we have performed the depth analysis of our samples using secondary ion mass spectroscopy and evaluated the concentration of  $F_4$ -TCNQ inside the sample by the method described in Ref. 37. Concentration of  $F_4$ -TCNQ is found constant throughout the sample which indicates perfect inter-diffusion of  $F_4$ -TCNQ. This indicates that quencher ( $F_4$ -TCNQ) is homogeneously dispersed in the host ( $Alq_3$ ), and Eq. (2) can be used for calculation of concentration of quencher. The ratio of  $I_0/I$  was calculated for all the samples and plotted against the molar concentration of  $F_4$ -TCNQ in Fig. 5. It can be seen from the figure that  $I_0/I$  scale linearly with the molar concentration. The quenching constant  $K_{sv}$  was calculated as the slope of this curve and found to be  $13.8 \text{ M}^{-1}$ . Zheng *et al.*<sup>12</sup> have measured the quenching constant for MEH-PPV and  $C_{60}$  to be  $2.5 \times 10^3 \text{ M}^{-1}$  and for MEH-PPV and TCM- $C_{60}$  to be  $1.8 \times 10^4 \text{ M}^{-1}$ . Quenching constant obtained in our system is three-four orders of magnitude smaller than the same obtained for MEH-PPV and  $C_{60}$  (or TCM- $C_{60}$ ). This signifies that  $F_4$ -TCNQ has weaker electron accepting capabilities from  $Alq_3$  than those in case of  $C_{60}$  when doped in MEH-PPV. In the report of Zheng *et al.*,<sup>12</sup> about one order of magnitude difference is observed for the quenching constant of TCM- $C_{60}$  and  $C_{60}$  due to their electron accepting capabilities. In these two cases, they have also observed formation of charge transfer complex. Further to clarify whether any collisional process is

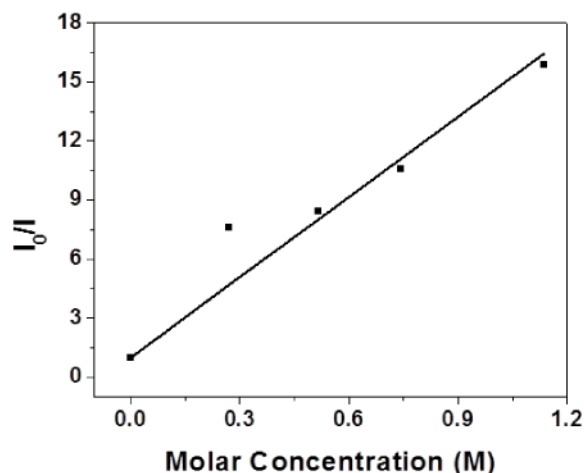


FIG. 5. Stern-Volmer plot for  $Alq_3$  quenching by  $F_4$ -TCNQ.

associated with the quenching mechanism, the TRPL spectrum was measured for all the samples and plotted in Fig. 6(a). It can be seen from this figure that excited state life time of  $Alq_3$  has reduced as  $F_4$ -TCNQ layer has been added in the sample; however, the excited state life time is independent of the concentration of  $F_4$ -TCNQ. Fig. 6(b) depicts the excited state life time as a function of  $F_4$ -TCNQ thickness and demonstrates the independence of excited state life time on its thickness. In the collisional (or dynamic) quenching mechanism, the ratio of intensities is equal to the ratio of excited state life time,<sup>24-27</sup> i.e.,

$$\frac{I_0}{I} = 1 + K_{sv} [Q] = \frac{\tau_0}{\tau}. \quad (3)$$

This implies that a plot of  $\frac{\tau_0}{\tau}$  as a function of  $[Q]$  should yield the same slope as the plot of  $\frac{I_0}{I}$  vs.  $[Q]$ . It is evident from the Fig. 6(b) that the value of slope is nearly zero. Even the excited state life time has decreased significantly (from 15.5 ns to approximately 3 ns) upon inclusion of  $F_4$ -TCNQ in the sample, excited state life time has not changed with changing thickness of  $F_4$ -TCNQ, however, at the same time, intensity has continuously decreased. Additionally, in case of dynamic quenching mechanism, the absorption spectrum does not change, in other words charge transfer complex does not form in ground state. Therefore, the quenching mechanism in the  $Alq_3$ - $F_4$ -TCNQ system cannot be associated to the dynamic type quenching mechanism, and the change in excited state life time may be ascribed as due to the formation of charge transfer complex between  $Alq_3$  and  $F_4$ -TCNQ. Other possible mechanism could be quenching due to the long range energy transfer from  $Alq_3$  to  $F_4$ -TCNQ. However, for a long range energy transfer process, the emission spectrum of donor ( $Alq_3$ ) should have an overlap with the excitation or absorption spectrum of acceptor ( $F_4$ -TCNQ). Fig. 6(c) depicts the emission spectrum of  $Alq_3$  and  $F_4$ -TCNQ absorption spectrum and these two spectra have negligible overlap which nullifies the possibility of quenching due to long-range energy transfer. Therefore, the quenching mechanism in the studied system can be associated to static type quenching. Steady state and transient PL analysis reveals that a stable charge transfer

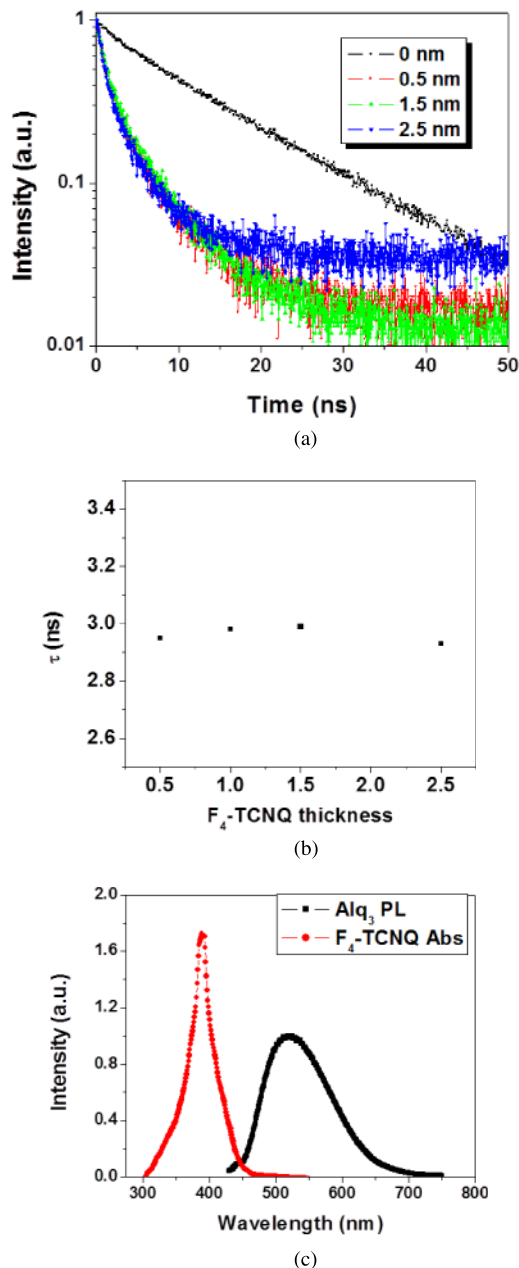


FIG. 6. (a) TRPL spectra of the samples with 0, 0.5, 1.5, and 2.5 nm thicknesses of  $F_4$ -TCNQ and 10 nm thickness of  $Alq_3$ . (b) Measured excited state life time as a function of  $F_4$ -TCNQ thickness as measured for the samples showing negligible change with variation of thickness. (c) PL spectrum of  $Alq_3$  (black squares) and absorption spectrum of  $F_4$ -TCNQ (red circles) showing negligible overlap between the two.

complex is formed between  $Alq_3$  and  $F_4$ -TCNQ in ground state and the quenching process is static type.

Stern-Volmer constant ( $K_{sv}$ ) is the product of bimolecular quenching rate constant ( $Q_b$ ) and the excited state life time in the absence of quencher ( $\tau_0$ ). The TRPL spectra of  $Alq_3$  were fitted with two exponential decay curves,

$$I = Ae^{-t/\tau_1} + Be^{-t/\tau_2}, \quad (4)$$

where  $\tau_1$  and  $\tau_2$  are the life time of two decay components and A and B are their contributions in PL decay. The values of  $\tau_1$  and  $\tau_2$  were found to be 3.6 ns and 15.5 ns, respectively, and their contributions A and B were found to be 6.4% and

93.6%, respectively. Generally, in case of  $Alq_3$ , only one decay component is observed, which has a decay time in the range of 15–16 ns.<sup>33</sup> However, some authors have also observed two decay components, in which contribution of one decay component is very small in comparison to the other decay component.<sup>34</sup> Since the contribution of  $\tau_1$  is very small in comparison to  $\tau_2$ , the value of  $\tau_2$  was used to calculate the bimolecular quenching constant. The bimolecular quenching constant ( $Q_b$ ) for  $F_4$ -TCNQ was found to be  $8.7 \times 10^8 M^{-1} s^{-1}$ .

Further,  $F_4$ -TCNQ has a very low sticking coefficient with most of the commonly used substrates; therefore, it tends to diffuse into the subsequent layers. SIMS is one of the most widely used techniques for the detection of diffusion. However, SIMS is a destructive technique and in that term it has a severe disadvantage. PL quenching studies have revealed that  $F_4$ -TCNQ molecules near  $Alq_3$  form a bimolecular charge transfer complex which is non-radiative. Corresponding bimolecular quenching constant was also found to be very high. Therefore, we have studied the diffusion of  $F_4$ -TCNQ using PL-spectroscopy. Second type of samples was fabricated for this study, in which  $\alpha$ -NPD layer was inserted between  $F_4$ -TCNQ and  $Alq_3$  and thickness of this layer was varied.  $\alpha$ -NPD has absorption spectrum centered at 380 nm and its absorption was found to be negligible at 405 nm, and the samples were excited with this wavelength. Further, we have also confirmed this by measuring the PL spectrum of  $\alpha$ -NPD with 405 nm as excitation wavelength.  $\alpha$ -NPD was also been selected due to its wide use as hole transport layer in OLEDs, which makes our device structure to be of practical importance. Diffusion of  $F_4$ -TCNQ through  $\alpha$ -NPD will lead to the quenching in  $Alq_3$ , thereby reducing the PL intensity of  $Alq_3$ . We have fabricated samples with 1, 2.5, and 5.5 nm thicknesses of  $F_4$ -TCNQ and for each sample, we have varied the thickness of  $\alpha$ -NPD. Figures 7(a)–7(c) show the PL spectrum of the samples with 1, 2.5, and 5.5 nm thicknesses of  $F_4$ -TCNQ and different thicknesses of  $\alpha$ -NPD. It can be seen from the figures that the PL intensity has the lowest value when the layer of  $\alpha$ -NPD was not present in the samples which may be ascribed by the direct contact of emitting ( $Alq_3$ ) and quenching ( $F_4$ -TCNQ) species. As the thickness of  $\alpha$ -NPD has increased, PL intensity has started to increase and after a certain thickness it saturates. This thickness has been found to be quite high (>15 nm) for all samples. Therefore, these data reflect towards the diffusion of  $F_4$ -TCNQ through  $\alpha$ -NPD layer and then,  $F_4$ -TCNQ caused the quenching of luminescence in  $Alq_3$  by exciton dissociation.

Further, for quantitative analysis, PL intensity was plotted as a function of  $\alpha$ -NPD thickness for the samples with 1, 2.5, and 5.5 nm thicknesses of  $F_4$ -TCNQ in Fig. 7. It can be seen from Fig. 8 that as the  $\alpha$ -NPD thickness has increased, the PL intensity was found to increase for all the samples. It can also be observed that the PL intensity is lowest for the samples with 5.5 nm thickness of  $F_4$ -TCNQ and highest for the sample with 1 nm thickness of  $F_4$ -TCNQ for same thickness of  $\alpha$ -NPD. This may be ascribed as due to the highest  $F_4$ -TCNQ density deposited in case of the sample with its 5.5 nm thickness. This will allow the higher density of  $F_4$ -TCNQ to be diffused into  $Alq_3$  layer and thus will have higher quenching of fluorescence. These data reflect that the

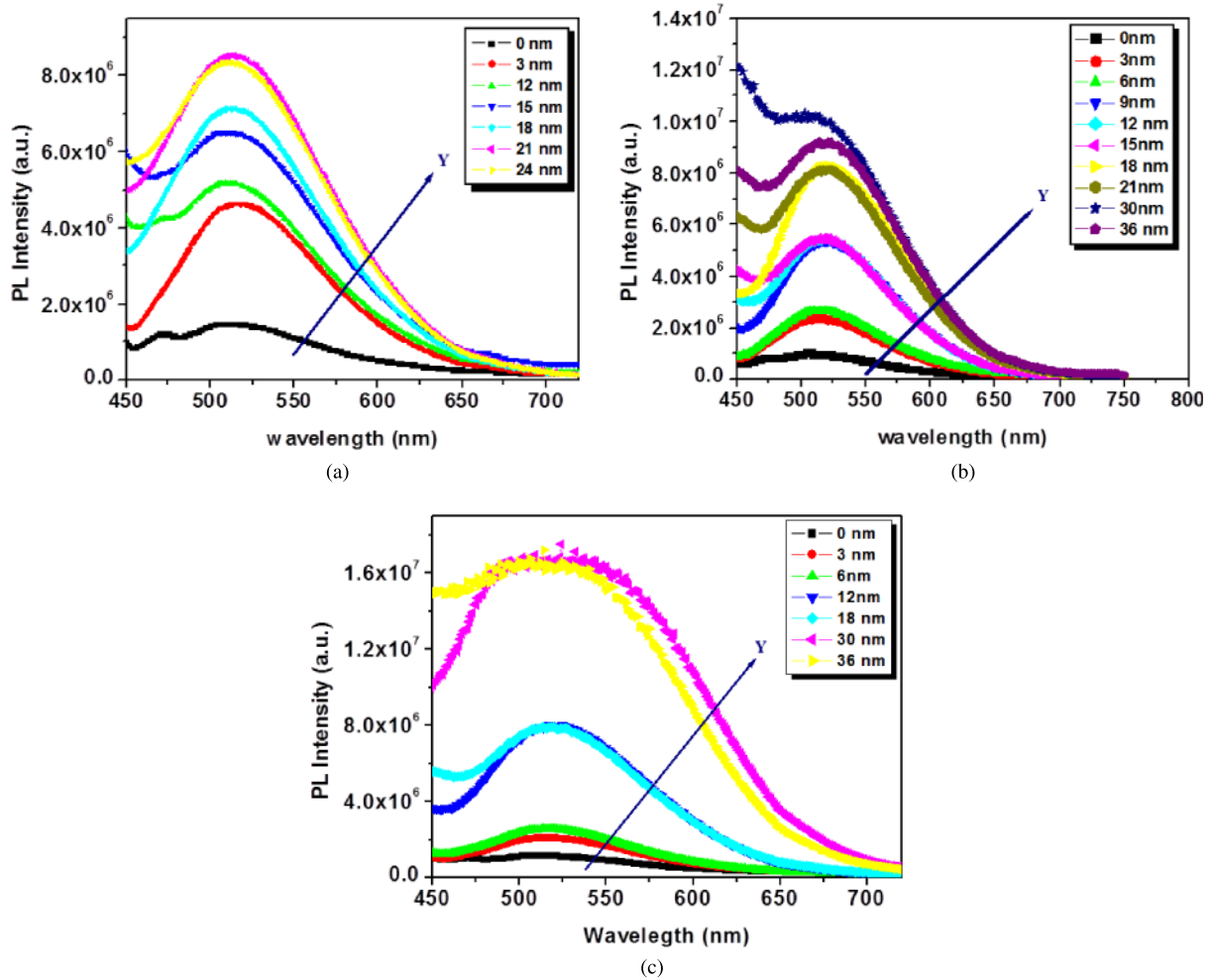


FIG. 7. PL spectrum of the samples with (a) 1 nm, (b) 2.5 nm, and (c) 5.5 nm thicknesses of  $F_4$ -TCNQ, for different thicknesses of  $\alpha$ -NPD spacing layer.

PL measurements on these samples have decent measure of distance and concentration dependence of  $F_4$ -TCNQ diffusion.

Further, we have calculated the quenching efficiency for these samples by using following equation:

$$Q.E.(r) = 1 - \frac{I(r)}{I_0}, \quad (5)$$

where  $I(r)$  is the peak PL intensity for the sample having a distance  $r$  between  $Alq_3$  and  $F_4$ -TCNQ, which means having

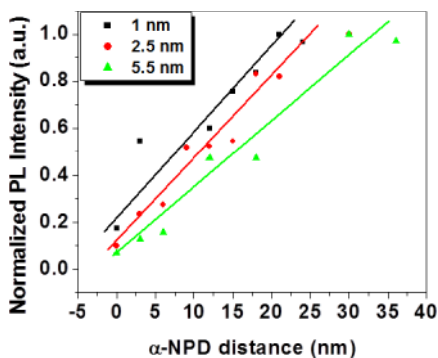


FIG. 8. Normalized PL intensity as a function of  $\alpha$ -NPD thickness for the samples with 1, 2.5, and 5.5 nm thicknesses of  $F_4$ -TCNQ.

$r$  thickness of  $\alpha$ -NPD,  $I_0$  is the peak intensity when  $F_4$ -TCNQ is at an infinite distance from  $Alq_3$ , which has been chosen as the saturation intensity of PL spectrum for all the samples. This quenching efficiency is directly proportional to the concentration of  $F_4$ -TCNQ present at that spatial position. Therefore, it provides a direct indication of  $F_4$ -TCNQ diffusion. The calculated quenching efficiency has been plotted as a function of the distance between  $F_4$ -TCNQ and  $Alq_3$  (in other words, as a function of  $\alpha$ -NPD thickness) in Fig. 9. Generally, the diffusion profile of a molecule with a constant source of diffusion at  $x = 0$  is governed by Gaussian distribution<sup>38,39</sup>

$$C(r) = C_0 \exp\left(-\frac{r^2}{L_d^2}\right), \quad (6)$$

where  $L_d$  is the diffusion length,  $C(r)$  the dopant present at a distance of  $r$ , and  $C_0$  the dopant present at  $x = 0$ . In case of quencher diffusion, diffusion length is related to a diffusion constant and time as  $L_d = 2\sqrt{Dt}$ , where  $D$  is diffusion constant and  $t$  the time and if we fix a duration of diffusion ( $t$  fixed), we can obtain a diffusion length. In our samples, we have performed the measurements after a fixed duration of time (1 h after the deposition of films) to compare the diffusion length.  $F_4$ -TCNQ concentration present at a distance  $r$ ,  $C(r)$ , is directly proportional to the quenching efficiency. Therefore,

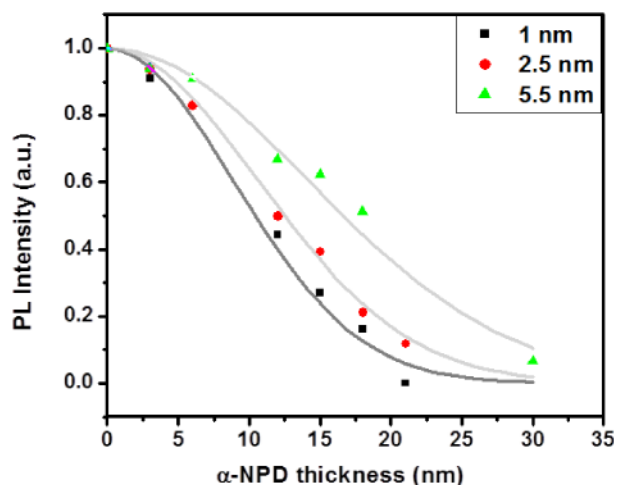


FIG. 9. Quenching efficiency (data points) as a function of  $\alpha$ -NPD thickness for 1, 2.5, and 5.5 nm thicknesses of  $F_4$ -TCNQ. Solid line shows the Gaussian fits, which were used to estimate the diffusion length for  $F_4$ -TCNQ.

the quenching efficiency data shown in Fig. 8 were fitted with a Gaussian distribution and good fits were achieved for diffusion lengths of 12.5, 15, and 20 nm for 1, 2.5, and 5.5 nm thicknesses of  $F_4$ -TCNQ, respectively. The reported values of  $F_4$ -TCNQ diffusion lengths measured using SIMS technique are 13, 15, and 18 nm for 1, 2.5, and 5.5 nm thicknesses of  $F_4$ -TCNQ, respectively.<sup>37</sup> These values match very closely to the values estimated by PL measurements.

We have also measured the time resolved PL spectrum for all the samples. All PL decay curves were found to possess one dominating decay component. This decay component was found to  $11.1 \pm 3.2$  ns,  $10.5 \pm 2.2$  ns, and  $10.8 \pm 2.1$  ns for samples with 1, 2.5, and 5.5 nm thicknesses of  $F_4$ -TCNQ, respectively. The averaging was performed for all the samples having different thicknesses of  $\alpha$ -NPD. The excited state life time was found to be independent of  $\alpha$ -NPD thickness as shown in Figs. 10(a)-10(c), which will vary the  $F_4$ -TCNQ diffused concentration interacting with Alq<sub>3</sub>. In the same figures, the ratio of intensities is also included which shows a significant decrease unlike the excited state life time with variation of  $\alpha$ -NPD thickness. According to Eq. (3), ratio of excited state life time and the intensity should be same in case of dynamic quenching mechanism. It is evident from the Fig. 10 that the slope of excited state life time ratio vs.  $\alpha$ -NPD thickness is nearly zero, while the ratio of intensity vs.  $\alpha$ -NPD thickness has higher slope. As the  $\alpha$ -NPD thickness is changed in the samples, the concentration of  $F_4$ -TCNQ mixed in Alq<sub>3</sub> changes according to Eq. (6). The change in concentration has led to change in intensity; however, the excited state life time remained nearly constant. This confirms the static quenching mechanism in this system.

Figure 11 shows the schematic illustration of our experiments. PL intensity has the largest value when the pristine fluorescent species is deposited on the substrates, and it drastically reduces with the insertion of the quencher layer. In our experiments, almost an order of magnitude decrease in PL intensity was observed. As we inserted an additional layer between the quencher and fluorophore, the PL intensity has started to increase. PL intensity is expected to reach its original

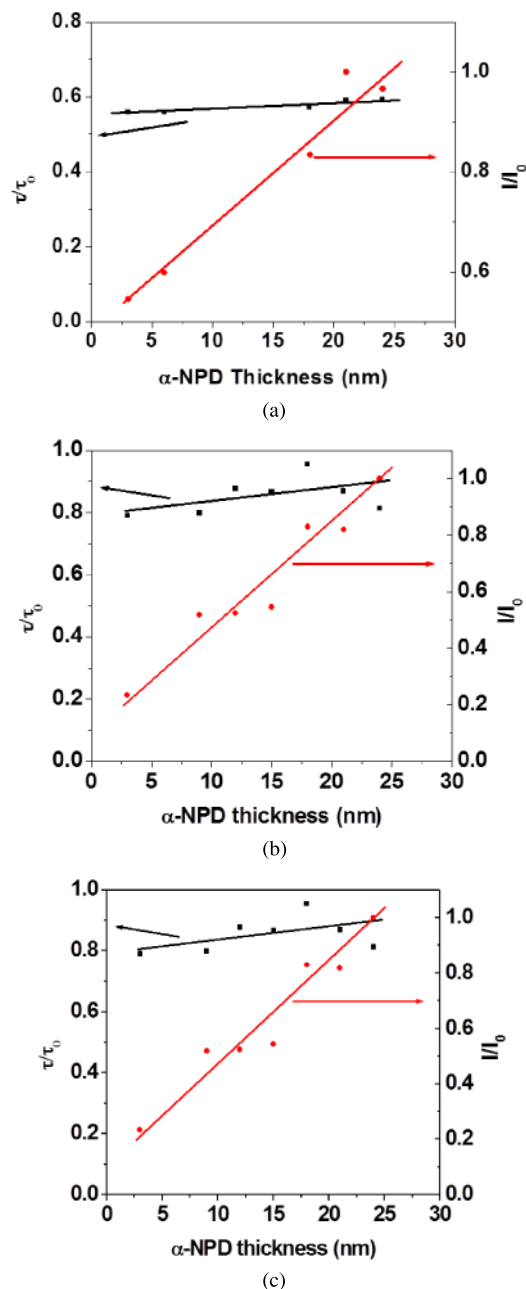


FIG. 10. Excited state life time normalized with the excited state life time of pristine Alq<sub>3</sub> as a function of  $\alpha$ -NPD thickness for the samples with (a) 1 nm, (b) 2.5 nm, and (c) 5.5 nm thicknesses of  $F_4$ -TCNQ. Corresponding ratios of intensities are also shown in all the figures.

value without the quencher layer with the insertion of additional layer because the quenching occurred due to the formation of charge transfer complex between quencher and fluorophore. This formation should be prohibited by the insertion of the additional layer. However,  $F_4$ -TCNQ diffuses through this layer and comes in the contact of fluorophore, where it forms a charge transfer complex. This restrained the PL intensity to recover its original value. The Gaussian curve in the Fig. 11 depicts the spatial  $F_4$ -TCNQ concentration  $C(x)$  in the samples. Further, increase in the thickness of the spacer layer increases the distance between quencher and fluorophore, thereby decreasing the diffused concentration of quencher. This decreases the amount of charge transfer between quencher

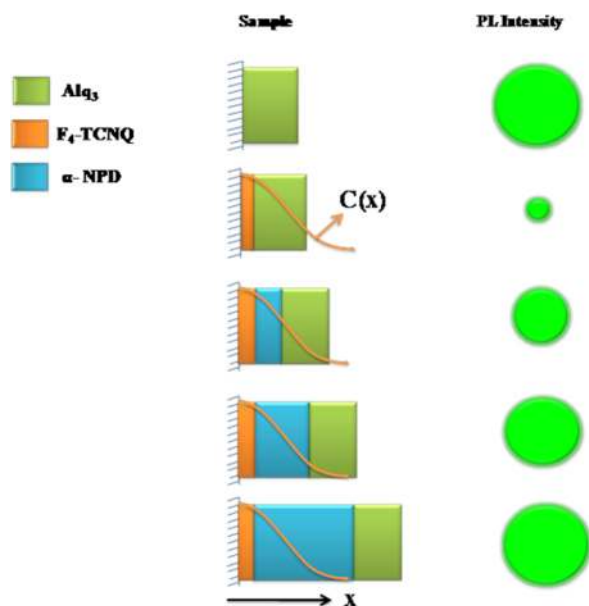


FIG. 11. Schematic illustration showing the variation of PL intensity for different samples. First sample is for pure Alq<sub>3</sub>, second has a thin layer of F<sub>4</sub>-TCNQ, and the rest are for different thicknesses of  $\alpha$ -NPD. The curve C(x) is showing the diffused concentration of F<sub>4</sub>-TCNQ.

and fluorophore and increases the PL intensity. Once the thickness of spacer layer has increased to a value greater than the diffusion length of quencher, the PL intensity of fluorophore attains its original value without the presence of quencher.

## CONCLUSION

Fluorescence quenching by F<sub>4</sub>-TCNQ was studied using PL spectroscopy. Static quenching mechanism was found responsible for the decrease in PL intensity of Alq<sub>3</sub> by F<sub>4</sub>-TCNQ. Stern-Volmer and bimolecular quenching constants were evaluated and found to be 13.8 M<sup>-1</sup> and 8.7 × 10<sup>8</sup> M<sup>-1</sup> s<sup>-1</sup>, respectively. Solid state diffusion of F<sub>4</sub>-TCNQ was studied through  $\alpha$ -NPD by fabricating samples having  $\alpha$ -NPD spacing layer between Alq<sub>3</sub> and F<sub>4</sub>-TCNQ. Diffusion lengths were estimated by calculating the quenching rate for different distances between Alq<sub>3</sub> and F<sub>4</sub>-TCNQ and found to be 12.5, 15, and 20 nm for 1, 2.5, and 5.5 nm thicknesses of F<sub>4</sub>-TCNQ, respectively. These results were found to be comparable to the measurements by SIMS technique.

<sup>1</sup>C. W. Tang and S. A. Vanslyke, *Appl. Phys. Lett.* **51**, 913 (1987).

<sup>2</sup>B. C. Krummacker, V. E. Choong, M. K. Mathai, S. A. Choulis, and F. So, *Appl. Phys. Lett.* **88**, 113506 (2006).

<sup>3</sup>J. H. Seo, J. H. Park, U. K. Kim, J. W. Hyung, K. H. Lee, and S. S. Yoon, *Appl. Phys. Lett.* **90**, 203507 (2007).

<sup>4</sup>A. R. Murphy and J. M. Frechet, *Chem. Rev.* **107**, 1066 (2007).

<sup>5</sup>G. Hughes and M. R. Bryce, *J. Mater. Chem.* **15**, 94 (2005).

<sup>6</sup>S. Oyston, C. Wang, G. Hughes, A. S. Batsanov, I. F. Perepichka, M. R. Bryce, J. H. Ahn, C. Pearson, and M. C. Petty, *J. Mater. Chem.* **15**, 194 (2005).

<sup>7</sup>P. Zhang, B. Xia, Q. Zhang, B. Yang, M. Li, G. Zhang, and W. Tian, *Synth. Met.* **156**, 705 (2006).

<sup>8</sup>J. Wang, F. Zhang, J. Zhang, W. Tang, A. Tang, H. Peng, Z. Xu, F. Teng, and Y. Wang, *J. Photochem. Photobiol., C* **17**, 69 (2013).

<sup>9</sup>O. A. Abdulrazzaq, V. Saini, S. Bourdo, E. Dervishi, and A. S. Biris, *Part. Sci. Technol.* **31**, 427 (2013).

<sup>10</sup>J. Mei, M. S. Bradley, and V. Bulović, *Phys. Rev. B* **79**, 235205 (2009).

<sup>11</sup>B. Pan, D. Cui, C. S. Ozkan, M. Ozkan, P. Xu, T. Huang, F. Liu, H. Chen, Q. Li, R. He, and F. Gao, *J. Phys. Chem. C* **112**, 939 (2008).

<sup>12</sup>M. Zheng, F. Bai, F. Li, Y. Li, and D. Zhu, *J. Appl. Polym. Sci.* **70**, 599 (1998).

<sup>13</sup>P. E. Shaw, H. Cavaye, S. S. Y. Chen, M. James, I. R. Gentle, and P. L. Burn, *Phys. Chem. Chem. Phys.* **15**, 9845 (2013).

<sup>14</sup>K. Boldt, S. Jander, K. Hoppe, and H. Weller, *ACS Nano* **5**, 8115 (2011).

<sup>15</sup>M. Pfeiffer, A. Beyer, T. Fritz, and K. Leo, *Appl. Phys. Lett.* **73**, 3202 (1998).

<sup>16</sup>J. Blochwitz, M. Pfeiffer, T. Fritz, K. Leo, D. M. Alloway, P. A. Lee, and N. R. Armstrong, *Org. Electron.* **2**, 97 (2001).

<sup>17</sup>X. Zhou, M. Pfeiffer, J. Blochwitz, A. Werner, A. Nollau, T. Fritz, and K. Leo, *Appl. Phys. Lett.* **78**, 410 (2001).

<sup>18</sup>M. Kröger, S. Hamwi, J. Meyer, T. Riedl, W. Kowalsky, and A. Kahn, *Org. Electron.* **10**, 932 (2009).

<sup>19</sup>J. S. Huang, C. Y. Chou, M. Y. Liu, K. H. Tsai, W. H. Lin, and C. F. Lin, *Org. Electron.* **10**, 1060 (2009).

<sup>20</sup>B. Maennig, M. Pfeiffer, A. Nollau, X. Zhou, K. Leo, and P. Simon, *Phys. Rev. B* **64**, 195208 (2001).

<sup>21</sup>A. Pal, S. Srivastava, R. Gupta, and S. Sapra, *Phys. Chem. Chem. Phys.* **15**, 15888 (2013).

<sup>22</sup>P. J. Goutam, D. K. Singh, and P. K. Iyer, *J. Phys. Chem. C* **116**, 8196 (2012).

<sup>23</sup>M. Lovelle, T. Mach, K. R. Mahendran, H. Weingart, M. Winterhalter, and P. Gameiro, *Phys. Chem. Chem. Phys.* **13**, 1521 (2011).

<sup>24</sup>M. Loumagne, R. Praho, D. Nutarelli, M. H. V. Werts, and A. Débarre, *Phys. Chem. Chem. Phys.* **12**, 11004 (2010).

<sup>25</sup>J. R. Lakowicz, *Principles of Fluorescence Spectroscopy* (Springer U.S., 2006), pp. 277–330.

<sup>26</sup>P. P. H. Cheng, D. Silvester, G. Wang, G. Kalyuzhny, A. Douglas, and R. W. Murr, *J. Phys. Chem. B* **110**, 4637 (2006).

<sup>27</sup>E. I. Zenkevich, T. Blaudeck, A. Milekhin, and C.v. Borczykowski, *Int. J. Spectrosc.* **14** (2012).

<sup>28</sup>P. Tyagi, A. Kumar, L. I. Giri, M. K. Dalai, S. Tuli, M. N. Kamalasanan, and R. Srivastava, *Opt. Lett.* **38**, 3854 (2013).

<sup>29</sup>L. Cosimbescu, A. B. Padmaperuma, and D. J. Gaspar, *J. Phys. Chem. A* **115**, 13498 (2011).

<sup>30</sup>J. S. Fletcher, N. P. Lockyer, and J. C. Vickerman, *Surf. Interface Anal.* **38**, 1393 (2006).

<sup>31</sup>G. Gillen and S. Roberson, *Rapid Commun. Mass Spectrom.* **12**, 1303 (1998).

<sup>32</sup>P. Wei, T. Menke, B. D. Naab, K. Leo, M. Riede, and Z. Bao, *J. Am. Chem. Soc.* **134**, 3999 (2012).

<sup>33</sup>C. W. Tang, S. A. Vanslyke, and C. H. Chen, *J. Appl. Phys.* **51**, 3610 (1989).

<sup>34</sup>R. Priestley, A. D. Walser, and R. Dorsinville, *Opt. Commun.* **158**, 93 (1998).

<sup>35</sup>P. Pingel and D. Neher, *Phys. Rev. B* **87**, 115209 (2013).

<sup>36</sup>C. Ungureanu and A. Airinei, *J. Med. Chem.* **43**, 3186 (2000).

<sup>37</sup>P. Tyagi, M. K. Dalai, C. K. Suman, S. Tuli, and R. Srivastava, *RSC Adv.* **3**, 24553 (2013).

<sup>38</sup>G. S. May and S. M. Sze, *Fundamental of Semiconductor Fabrication* (Wiley Publishing, 2004), Chap. 6.

<sup>39</sup>J. D. Plummer, *Silicon VLSI Technology: Fundamentals, Practice and Modeling* (Pearson Education, 2009), Chap. 7.

Journal of Chemical Physics is copyrighted by AIP Publishing LLC (AIP). Reuse of AIP content is subject to the terms at: <http://scitation.aip.org/termsconditions>. For more information, see <http://publishing.aip.org/authors/rights-and-permissions>.